Evaluation of Aromatic Oxidation Reactions in Seven Chemical Mechanisms with an Outdoor Chamber

Harshal M. Parikh[a], Harvey E. Jeffries[a], Ken G. Sexton[a], Deborah J. Luecken[b], Richard M. Kamens[a], William Vizuete[a,□]

[a]Department of Environmental Sciences and Engineering, School of Public Health, University of North Carolina, 1302 MHRC, CB 7431, Chapel Hill, NC 27599-7431, USA□

[b]U.S. Environmental Protection Agency, 109 T.W. Alexander Drive, Mail Drop E243-03, Research Triangle Park, NC 27709, USA

□Corresponding author. Tel.: 919 966 0693; fax: 919 966 7911. E-mail address: vizuete@unc.edu

Email addresses: harshal@email.unc.edu (Harshal M. Parikh), harvey@email.unc.edu (Harvey E. Jeffries), kgsexton@email.unc.edu□(Ken G. Sexton), luecken.deborah@epa.gov (Deborah J. Luecken), kamens@unc.edu (Richard M. Kamens), vizuete@unc.edu (William Vizuete)

Environmental Context.

Aromatic hydrocarbons in the atmosphere can form large amounts of ozone, contribute to $PM_{2.5}$, and can be hazardous air pollutants. Regulatory air quality models (AQMs) used to develop strategies to reduce ozone and other pollutants must be able to accurately predict ozone from aromatic hydrocarbons in urban areas. In urban areas major sources of aromatic hydrocarbons are gasoline and diesel powered vehicles and are targets of control strategies justified using AQMs. These findings show that representation of aromatic chemistry in AQMs is insufficient to accurately predict the chemical production of ozone.

Abstract

Simulations using seven chemical mechanisms are intercompared against O_3, NO_x, and hydrocarbon data from photooxidation experiments conducted at the University of North Carolina outdoor smog chamber. The mechanisms include CB4-2002, CB05, CB05-TU, a CB05 variant with semi-explicit aromatic chemistry (CB05RMK), SAPRC07, CS07, and MCMv3.1. The experiments span a variety of aromatics, unsaturated dicarbonyls, and VOC mixtures representing a wide range of urban environments with relevant

hydrocarbon species. In chamber simulations the sunlight is characterized using a new solar radiation modeling software. A new heterogeneous chamber wall mechanism is also presented as a revised model of the chemical processes occurring on chamber walls.

Simulations from all mechanisms, except MCMv3.1, show the median peak O_3 relative error of less than 25% for both aromatic and VOC mixture experiments. Although MCMv3.1 largely overpredicts peak O_3, it performs relatively better in predicting the peak NO_2 compared to other mechanisms. For aromatic experiments, all mechanisms except CB4-2002, largely underpredict the NO-NO_2 crossover time and over-predict both the absolute NO degradation slope and the slope of NO_2 rise. This suggests a major problem of faster and earlier NO to NO_2 oxidation rate across all the newer mechanisms. Results from individual aromatic and unsaturated dicarbonyl experiments illustrate the unique photooxidation chemistry and O_3 production of several aromatic ring-opening products. The representation of these products as a single mechanism species in CB4-2002, CB05, and CB05-TU is not adequate to capture the O_3 temporal profile. In summary, future updates to chemical mechanisms should focus on chemistry of aromatic ring-opening products.

Keywords: Chemical mechanisms, Ozone, Aromatics, SAPRC, MCM, CB05

1. Introduction

Volatile organic compounds (VOC) in the presence of nitrogen oxides (NO_x) undergo photooxidation leading to the formation of photochemical smog. Aromatic species contribute approximately 10% [1] to 20% [2] of the global anthropogenic non-methane VOC emissions. Specifically, the major sources of aromatic hydrocarbons in urban VOC mixtures are gasoline and diesel powered vehicle exhaust and solvent usage. Emissions of aromatics play a key role in several of the most widespread and harmful air pollution problems in the U.S. and throughout the world. Ozone pollution has been estimated to be the largest cause of preventable, premature mortality across the world, and aromatic hydrocarbons substantially contribute to ozone production on a regional scale and play a key role in an urban polluted environment through complex tropospheric chemistry [3, 4]. Aromatic hydrocarbons are also precursors to secondary organic aerosols [5-7], and thus contribute to PM2.5 concentrations, which can cause cardiovascular and pulmonary illness, premature mortality as well as environmental degradation. Several of most widely emitted compounds, including toluene and xylene isomers, are also hazardous air pollutants which are known to cause a variety of cancer and noncancerous health effects [8]. Because of the role that aromatics play in these multiple aspects of human and environmental health, it is critical to understand the chemical fate of aromatic compounds.

Air quality model (AQM) simulations are extensively used to predict and study the transport, chemistry, and deposition of ozone and other air pollutants. For ozone pollution, a regional scale AQM is commonly used as a regulatory tool to demonstrate attainment below federally specified levels. The representation of complex tropospheric chemistry and photolysis in AQMs is described in a chemical mechanism [9]. Several

chemical mechanisms have been developed and used to represent atmospheric chemistry with either explicit or semi-explicit reactions (e.g., 12,600 reactions and 4,500 species) or condensed mechanisms (e.g., 81 reactions and 33 species).

Explicit/Semi-explicit mechanisms represent in great detail the atmospheric oxidation of a large number emitted VOC, including aromatic hydrocarbons. For example, the Master Chemical Mechanism (MCMv3) represents the semi-explicit chemistry of 124 emitted VOC species [10, 11]. MCM has been extensively used in three-dimensional Lagrangian chemistry-transport AQM [3, 12, 13]. Although its use in Eulerian grid-based AQM has been limited due to high computational requirements, a recent study has implemented MCM for ozone predictions in the Community Multiscale Air Quality Modeling System (CMAQ), a regional-scale Eulerian model [14].

Condensed chemical mechanisms can be categorized into lumped species mechanisms and the Carbon Bond (CB) approach. Lumped species mechanisms, e.g., SAPRC07 [15] use a single lumped mechanism species to represent a group of explicit chemical entities. The groups are based on the gas-phase reactivity of the individual entities. In the CB approach most organics are grouped according to bond type. This structural lumping technique categorizes the reactions of similar carbon bonds [16, 17].

Further, mechanisms also differ in representations of complex aromatic and biogenic species chemistry. Particularly for aromatics, the proposed pathways of oxidation chemistry, reaction rate constants, and species cross section (CS) and quantum yields (QY) are uncertain and incomplete [2]. Several recent studies have identified products and mechanisms of aromatic species degradation [18-20]. Additional complexity arises from representations of carbonyl products formed from aromatic ring-opening routes. Many of these individual products are highly polar, photolabile [21], and react further in ways that are different from better understood alkane and simple alkene monofunctional products [22].

Because of the complex differences in representation of aromatic hydrocarbons, and their intimate integration with the rest of the entire photochemical system, it is difficult to understand how these differences affect the overall chemistry. Are the schemes really that much different in their overall concentration predictions? Do these differences result in significant differences in some of the most important pollutants that affect human health and the environment, such as ozone?

The overall objective of this study is to address these questions by systematically evaluate seven existing chemical mechanisms that range from explicit to condensed using 35 years of observations from outdoor chamber experiments conducted at University of North Carolina (UNC), with the Mollner et al. (2010) rate constant and updated cross section (CS)/quantum yields (QY) of inorganic and organic photolytic species. Specifically, we seek to evaluate mostly the aromatic chemistry component of these mechanisms and its interactions with the overall mechanism using experiments with pure aromatic species and with different urban and vehicle exhaust mixtures that contain a significant fraction of aromatic species.

Although the UNC chamber experiments have been previously used to develop and evaluate earlier versions of the CB mechanism, they have never been used to intercompare the latest versions of chemical mechanisms available in regulatory AQMs. Comparison of observed and predicted O_3, NO, NO_2, VOC, and carbonyl temporal profiles from specific experiments and overall measures of performance allow us to suggest potential problem formulation differences for the aromatic chemistry amongst mechanisms. This analysis also can show common biases that may be present across all mechanisms. In addition, four experiments with injections of different 1,4-unsaturated dicarbonyls and NO_x are modeled with all seven mechanisms. These dicarbonyls are known to be products of aromatic photochemical oxidation and react further with different pathways based on the chemical structure and location of the unsaturated double bond [22, 23]. Modeling this new data allow us to specifically study the performance of chemical mechanisms relative to O_3 forming potential of known intermediate products of aromatic oxidation chemistry.

These modeling results are used in identification of important generalizations, distortions and deletions within current chemical mechanisms that may be impacting the ability of the mechanism to accurately characterize overall atmospheric photochemistry. These results serve as a guide to develop future condensed mechanisms for aromatics. This study is the first to our knowledge, that collectively evaluates seven gas-phase chemical mechanisms against a comprehensive set of aromatics, unsaturated dicarbonyl intermediates, and VOC mixtures experiments conducted in a single outdoor chamber. It thus provides a framework for analyzing, comparing and contrasting alternate techniques for representing complex photochemistry used in regulatory AQMs.

2. Experimental

Smog chamber data have been extensively used to evaluate and intercompare gas-phase chemical mechanisms as they provide a controlled environment, where the initial concentrations of VOC and NO_x are known and the time-varying concentrations of VOC, NO_x, O_3 and other secondary species concentrations can be monitored with precision [15, 21, 24, 25]. Because smog chambers reduce many of the uncertainties encountered in evaluations against ambient measurements, they provide an ideal platform for mechanism intercomparison, and allow us to address specific shortcomings due to generalizations and deletions. Similar biases and problems across mechanisms when comparing simulated and observed concentrations can also help explore missing reaction pathways. From a regulatory policy standpoint, the limitations and applicability of mechanisms under different gas-phase conditions can be fully evaluated.

All the experiments modeled for this study were carried out in the UNC 300,000-L dual gas outdoor chamber located in Chatham County, North Carolina. Two chambers, side by side, allow us to compare two experiments, under different initial species injections, at the same time. In each experiment, background concentrations of NO_x, O_3, and VOC were measured at the minimum. Detailed descriptions of the chambers and measurement instruments employed are available [25]. Based on the initial injections, Table 1 shows the

classification of 68 aromatic and mixture experiments used in this study. This table does not include additional chamber experiments (with background VOC and simple species like CO, HCHO, methane, ethene, propene, and acetaldehyde) used to perform chamber characterization and formulate the chamber auxiliary mechanism. In the supplementary material Table S1 shows the carbon fraction of individual species for all test synthetic urban mixtures. These urban mixtures each contain 16 to 54 species, ranging in varying complexity from simple alkanes/alkenes to various carbonyls and aromatics [26, 27]. To minimize chamber artifact effects, the concentration of reactants injected into the UNC chamber and the resulting VOC/ NO_x ratio tend to be fairly high. NO_x concentrations ranged from 0.2 to 0.6 ppm and initial VOC/ NO_x ratios are often 4:1 to 20:1. A detailed table showing initial injection concentrations for all modeled experiments is shown in the supplementary material Table S2.

Outdoor chambers exhibit temperature, light intensity, and relative humidity characteristics that are more representative of the open atmosphere. It is important to accurately represent day-to-day variations in these meteorological parameters, particularly the chamber actinic flux used in the computation of photolysis rates. For each experiment the chamber site's broadband Total Solar Radiation (TSR) and broadband Ultra Violet (UV) radiometers measure the time profile of surface TSR and UV horizontal irradiance. A broadband model [28] is used to simulate the TSR and UV radiation received at the chamber on a given day and accounts for atmospheric properties such as atmospheric pressure, total ozone column, total water vapor column, type of aerosol, aerosol optical density in stratosphere and troposphere, scattering properties, and relative humidity changes during the day. Finally, we account for the presence and nature of cloud cover through troughs and crests in observed TSR and UV transmission values.

Using the TSR and UV cloud transmissions from the broadband model and atmospheric properties, the time profile of surface spectral spherical irradiance (actinic flux) is computed outside the chamber. The time profile of actinic flux inside the chamber is computed every four minutes using the outside flux and a Teflon film transmission model, chamber geometry model, and a chamber reflective floor model. Both the outside and inside direct, diffuse, and reflective components of the total spectral irradiance predictions have been extensively tested using measurements taken with a Licor 1800 spectroradiometer. As an example, Figure S1 in the supplementary material shows the modeled global interval-averaged actinic flux inside the chamber for June 26, 1997 at three different times during the day. Once the in-chamber actinic flux has been calculated, the sunlight model computes the in-chamber photolysis rates every 4 minutes using Equation 1.

$$j = \sum_{\lambda_m}^{\lambda_n} j_\lambda d\lambda = \sum_{\lambda_m}^{\lambda_n} A_\lambda \sigma_\lambda \Phi_\lambda d\lambda \qquad (1)$$

where, j is the photolysis rate for a particular reaction (units of min^{-1}) and j_λ is the spectral photolysis rate (units of min^{-1}-nm^{-1}) computed as a product of spectral actinic flux (A_λ) with units of photons-cm^{-2}-min^{-1}-nm^{-1}, molecular absorption cross-section unique for each photolytic species (σ_λ) with units of cm^2-$molecule^{-1}$ and process quantum yield (Φ_λ), a unitless quantity, which is the fraction of absorbing molecules at λ that proceed by a

certain reaction pathway.

Figure S2 in the supplementary material shows the simulated photolysis rates for NO_2, O_3, and HCHO on June 26, 1997. The chamber sunlight model captures both the diurnal pattern of photolysis rates and the effects of clouds through sharp troughs and crests throughout the day.

2.1 Chemical mechanism descriptions

Seven mechanisms were used to model the chamber experiments:

- Mechanisms with CB approach include the 2002 update of CB4 [16] indicated as CB4-2002 [29], a 2005 update of the CB mechanism indicated as CB05 [17], CB05 with new toluene update (CB05TU) [30], and CB05 with new condensed toluene and xylene mechanism (CB05RMK) [5]. In the initial testing of CB05RMK lower NOx concentrations were used than tested here. These experiments ranged from 0.12 to 0.22 NOx and 0.7 to 3.5 ppmC of toluene and generated 0.22 to 0.45 ppm of O_3. Model performance was reasonable with the O_3 being over predicted by only 0-30%.

- Mechanisms with lumped species approach include the latest version of SAPRC mechanism called SAPRC07 [15] and a condensed version of the SAPRC07 mechanism designated as CS07 [31].

- Master chemical mechanism (MCM) that represents an explicit chemical mechanism. The latest version of this mechanism designated as MCMv3.1 [32] is included in this study.

All the above mechanisms have been previously evaluated against data from either a single or a number of outdoor smog chambers [5, 15, 21, 24, 29, 30]. The mechanism evaluations, particularly for CB and SAPRC, follow a hierarchy of species approach [16]. Recent updates (e.g., CB05TU, CB05RMK, SAPRC07) have been primarily in the aromatic subparts of these mechanisms, in an attempt to improve ozone and secondary organic aerosol (SOA) predictions in urban areas.

All of the reaction rates in the mechanisms are implemented in the form originally proposed by the mechanism developer with one exception. In all mechanisms, the rate constant for the radical chain-terminating reaction $OH + NO_2 \rightarrow HNO_3$ has been changed to that be consistent with a recent study [33]. This is a major update to a reaction that is known to control the concentration of OH, the dominant oxidant in the atmosphere, and significantly affect ozone concentrations. Regional-scale AQM simulations with the new rate show 10 to 12 ppb higher ozone relative to IUPAC rate-constant recommendation and the simulations show a roughly 10% increase in ozone concentrations in regions of high ozone. An analysis of the substitution of this rate in SAPRC07 showed that the modified mechanism reproduced smog chamber data sufficiently close to the original mechanism that no changes to other reactions or products were needed [33]. While our general intent was to compare the alterative mechanisms "as is", neglecting the large impact of the new $OH + NO_2$ reaction could distort the NO_x cycling and increase

uncertainty in the comparison with smog chamber data, so we have chosen to limit the harmonization to this one reaction.

The CS/QY for all □7 inorganic and major organic photolytic species are updated and set to also be consistent across all mechanisms. The updating of these parameters, particularly the reaction rate constant update of a major radical termination reaction, requires new chamber characterization tests and formulation of a new auxiliary mechanism. This effort is described in detail in the next section.

2.2 Chamber auxiliary mechanism

It is well recognized that chamber walls have an effect on gas-phase experiments and is true for all chambers [9, 24, 29, 34-36]. Surface mediated reaction of nitrogen oxides and nitrogen acids occur in wall-absorbed water layer resulting in the creation of nitrous acid (HONO), which is emitted from the walls back into the gas-phase. HONO when photolyzed becomes a source of OH radicals and NO. Chamber walls also provide a place for the deposition and absorption of different gas-phase species.

To use smog chamber to evaluate an atmospheric chemical mechanism, you must include a set of chamber-dependent reactions that describe the above processes, known as the auxiliary mechanism, which are appended to the principal reaction mechanism that is being tested. The auxiliary mechanism also includes reaction of measured background VOC, treated as a mixture of the rural background air in Pittsboro, Chatham County North Carolina. Effects of background VOC are minimal and have been extensively tested previously with background VOC and NO_x experiments [37].

The existence and magnitude of wall processes is determined by conducting chamber characterization experiments. These experiments only include chemical systems that are well understood and can be represented by explicit chemical mechanisms (e.g. CO/ NO_x, HCHO/ NO_x, CH_4/ NO_x). For the UNC chamber an auxiliary mechanism was proposed in 2002 by Jeffries et al. (2002). Yarwood et al. (2005) updated the UNC wall reaction mechanism based heavily on CO/ NO_x characterization experiments. Although CO is useful as a characterization experiment; one problem at UNC chambers has been the formation of an iron carbonyl complex in the CO tank that is highly reactive when injected in the chamber. For this reason, we reverted to the auxiliary mechanism developed by Jeffries et al. (2002), that puts less weight on CO characterization experiments. Table 2 shows the auxiliary mechanism developed for this study.

Select characterization experiments used to formulate this mechanism are shown in Figures S4-S10 in the supplementary material. The explicit mechanisms for CO, CH_4, HCHO, acetaldehyde, ethene, and propene with updated rate constants and CS/QY are used as the principal reaction mechanisms. The biggest impact on the magnitude of chamber radical source is from the inclusion of the newer, reduced rate constant for radical termination reaction, OH + NO_2 [33]. This reduction means a light-dependent "missing" HONO source, that was part of the auxiliary mechanism developed by Jeffries et al. (2002) (as shown in reaction 17 - Table 2), is no longer required. Further, the OH + NO_2 rate constant in all seven chemical mechanisms is changed to maintain consistency

in required chamber radical sources between characterization experiments and aromatic/VOC mixture experiments.

In addition to the auxiliary mechanism, each experiment has unique injection values of initial wall water and initial HONO. These are dependent on the amount of time the chamber is vented with dry air before the experiment and recent history of experiments conducted in the chamber prior to that experiment.

2.3 Hydrocarbon speciation and chamber simulations

Modeling smog chamber experiments with different mechanisms requires assignment of injected VOC species to appropriate mechanism species. For MCMv3.1, a majority of VOCs injected in the chamber were treated explicitly. Certain species that were not present in the MCM, were assigned the closest surrogate species. A list of these species and their surrogates is shown on Table S3 in the supplementary material. For Carbon Bond and SAPRC mechanisms, special programs were developed that uses a published speciation database [38]. The database includes speciation information for all the VOC species injected in the chamber.

The chemical kinetic solver Morpho is used to solve the gas-phase chemistry for all mechanisms [39]. Much of the data needed for input to the simulation system is in the form of ASCII text files that has a collection of data segments with different time-base associated with the operation of different sampling instruments. In all, 68 experiments are simulated with seven different chemical mechanisms and the simulation results compared with NO, NO_2, O_3, and limited primary and secondary VOC data.

2.4 Measures of results

In addition to comparing observed temporal profiles of NO, NO_2, and O_3 against simulated values for selective experiments; it is necessary to compute different overall measures of results for all experiments. We selected one time of recognizable event (NO-NO_2 crossover time), three slopes (NO, NO_2, and O_3), and two maximum mixing ratios (i.e., NO_2 and O_3 maximum) as measures to be compared between observations and simulation results for each experiment. These measures are important indicators of the evolution of atmospheric photochemistry and are all described in Figure S3 [40]. For example, all the indicated measures are reported in the form of relative error computed using Equation 2.

$$\text{error} = (\text{model} - \text{data})/\text{data} \qquad (2)$$

3. Results and Discussion

3.1. Mechanism inter-comparison: Experiments with aromatics

Results from two experiments conducted on August 1, 1983 in the dual outdoor UNC smog chamber are presented in detail. In one isolated half of the chamber (indicated as

red side) 4 ppmC toluene/0.373 ppm NO_x is injected and 2.6 ppmC o-xylene /0.373 ppm NO_x is injected in the other isolated half of the chamber (indicated as blue side). Figures 1 and 2 show the comparison of observed O_3, NO, and NO_2 versus simulated results for the red and blue side of the chamber for all seven mechanisms.

On August 1 both the CB4-2002 and CB05 mechanisms tend to underpredict ozone and predict slow NO to NO_2 conversion, leading to higher modeled NO- NO_2 crossover times. All the remaining mechanisms tend to underpredict modeled NO- NO_2 crossover times, indicating higher reactivity earlier in the day and except CB05TU, tend to over-predict final ozone (Figure 1). One characteristic feature of toluene experiments is the "hockey stick" like trend for O_3. In Figure 2, the o-Xylene experiment shows a different observed O_3 profile. In this experiment the ozone concentrations have a continued rise for a few hours after mid-day (at a substantially lower slope than the initial rise) and starts dropping typically after 1500 local daylight time (LDT). All mechanisms are capable of predicting this trend as shown in Figure 2. For this experiment, CB05, CB05TU, SAPRC07, and CS07 tend to under-estimate the NO- NO_2 crossover times. Also, CB4-2002, CB05, and CB05TU underpredict O_3 compared to the remaining set of mechanisms and overall CB05RMK performs the best for this particular experiment.

Figure 3 shows temporal profile plots for an experiment performed on August 03, 1995, with 9 ppmC 1,3,5-TMB/0.629 ppm NO_x injection for four mechanisms. The observed O_3 profile for 1,3,5-TMB shows a rapid rise initially, then a decline between approximately 0900 to 1100 LDT and sharp rise again till the end of the day. The simulations from both the Carbon Bond mechanisms fail to reproduce this temporal profile. The SAPRC07 and MCMv3.1 are able to reproduce this behavior, but both overpredict O_3.

Figures 4 (a), (b), and (c) show the measured toluene, o-xylene, and 1,3,5- TMB degradation against predicted values for the three experiments described above. For toluene, all mechanisms show faster initial decay and slower late-afternoon decay when compared against the solid observed decay. For o-xylene, the results are similar to toluene, except for the first two hours of the experiment that shows slower decay for all mechanisms. For 1,3,5- TMB, the late-afternoon decay is severely underpredicted in all mechanisms consistent with the inability to predict sharp O_3 rise in the late afternoon (Figure 3).

Figure 5 shows the measures of results, as discussed in section 2.4, for all aromatic experiments. Peak O_3 is slightly underpredicted in most experiments for CB4-2002, CB05, and CB05TU mechanisms. O_3 is slightly overpredicted for CB05RMK, SAPRC07, and CS07. MCMv3.1 largely overpredicts O_3 with a median of approximately 50% relative error (Figure 5 (a)). Figure 5 (b) shows that NO- NO_2 crossover times are mostly underpredicted in all mechanisms, indicating early simulated NO to NO_2 conversion compared to actual observations. This underprediction is particularly severe in CB05TU. The peak NO_2 is slightly underpredicted for most experiments by all mechanisms except MCMv3.1, which shows a slight over-prediction for most experiments (Figure 5 (c)). Figures 5 (d), (e), and (f) show the errors in slopes for O_3,

NO, and NO_2. Positive relative errors for both absolute NO degradation slope and NO_2 rise indicate faster prediction of NO to NO_2 conversion from all mechanisms except CB4-2002 (Figures 5 (e) and (f)). The median relative error for O_3 slope (Figure 5 (d)) is fairly close to the zero error line for all mechanisms.

3.2. Mechanism inter-comparison: Experiments with VOC mixtures

Figure 6 shows the measures of results for all VOC mixture injection experiments. Peak O_3 is generally over-predicted by all mechanisms except CB4-2002 (Figure 6 (a)). Similar to aromatic experiments, the NO- NO_2 crossover times are underpredicted in all mechanisms (Figure 6 (b)). Figure 6 (c) shows considerable scatter in the peak NO_2 relative error. In general the medians of the relative error in peak NO_2 for all mechanisms, except MCMv3.1, are negative indicating lower simulated peak NO_2 compared to observed data. Both the NO and NO_2 slopes (Figure 6 (e) and (f)) from all mechanisms do not show a particular bias towards positive values as was seen in aromatics (Figures 5 (e) and (f)).

3.3. Ozone predictions from unsaturated dicarbonyls

As seen from observed O_3 temporal profiles in Figures 1-3, the presence of extra methyl groups on the aromatic ring results in different trends in O_3 behavior particularly later in the day. This is primarily due to the distribution of intermediate ring-opening unsaturated dicarbonyl oxidation products formed from different aromatic oxidation systems. Each of the intermediate products undergoes further oxidation and several of these species can act as temporary NO_2 sinks and can decompose to release NO_2 later in the day at higher temperatures. Although the complete identification of all intermediate products is an active research area, several important intermediates have been identified. It has been shown that 1,4-butenedial is a major intermediate product from toluene, 4-oxo-2-pentenal is a major intermediate product from o-xylene, and 3-hexene-2,5-dione is a major intermediate product from 1,3,5-TMB oxidation systems [41]. Sub-parts of chemical mechanisms that represent ring-opening product oxidation chemistry are tested using a total of four experiments: one experiment with 1 ppm butenedial/0.66 ppm NO_x injection, two 4-oxo-2-pentenal experiments, one with 0.81 ppm and another with 1.5 ppm injection along with 0.66 ppm NO_x, and one experiment with 0.95 ppm 3-hexene-2,5-dione with 0.66 NO_x injection.

Figure 7 shows the observed and modeled NO, NO_2, and O_3 profiles for both the red and blue side of the chamber. The CB05TU mechanism (like the CB05 mechanism) uses a single model species called "OPEN" to represent all the ring-opening products from aromatic oxidation. This highly condensed representation results in prediction of lower O_3 compared to observations. CB05RMK has semi-explicit representations of both butenedial and 4-oxo-2-pentenal resulting in better predictions for O_3 when compared to observations. Both SAPRC07 and MCMv3.1 over-predict O_3, but are unable to match the temporal profile. Figure 8 show the observed and modeled NO, NO_2, and O_3 profiles for the 3-hexene-2,5-dione experiment conducted on the blue side of the chamber. Once again both SAPRC07 and MCMv3.1 perform fairly well. Both CB05TU and CB05RMK underpredict O_3 largely due to lack of explicit or semi-explicit representation of 3-hexene-2,5-dione. The oxidation of this particular ring-opening product is fairly unique and possibly largely responsible for the O_3 behavior in 1,3,5-TMB/ NO_x oxidation

systems.

3.4. Discussion

3.4.1. Aromatics

It is clear from observed O_3 profiles for toluene, xylene, and 1,3,5-TMB (Figure 1, 5 and 6) that the oxidation chemistry of first-generation ring-opening products differs greatly and influences O_3 production in unique ways. Representation of these products has been a ongoing challenge for condensed mechanisms. The inherent constraint in formulation of CB4-2002, CB05, and CB05TU is the representation of these products as a single mechanism species called "OPEN". For 1,3,5-TMB this constraint also partly arises from loss of information due to the representation of this primary aromatic as xylene and a single carbon alkane (PAR) mechanism species. CB05RMK includes semi-explicit representations of certain unsaturated dicarbonyl ring-opening products (e.g., 1,4-butenedial, 4-oxo-pentenal and 2-methyl-2,4-hexadienedial). These species are representative of a spectrum of ring-opening products, with each semi-explicit species representing the unique oxidation chemistry associated with a particular group of ring-opening products. For the CB05RMK mechanism this results in better predictions of peak O_3 (Figure 5 (a)), NO- NO_2 crossover times (Figure 5 (b)), and temporal profile of O_3 in unsaturated dicarbonyl experiments (Figures 7 (a) and 8 (a)). In general, SAPRC07 performs well for both 1,3,5-TMB (Figure 3 (c)) and unsaturated dicarbonyl experiments (Figures 7 (c) and 8 (c)) due to three lumped representations of ring-opening products namely AFG1, AFG2, and AFG3. MCMv3.1 uses explicit species to represent ring-opening products and not surprisingly also performed well (Figures 7 (d) and 8 (d)), but like SAPRC07 it overpredicts ozone for the butenedial and oxopentenal experiments. The measures of results for aromatics (Figure 5) in general indicate the problem of faster and earlier simulated NO to NO_2 conversion particularly with the newer CB, SAPRC, and MCM mechanisms. This overall NO to NO_2 conversion rate helps with simulating rapid O_3 production as is typically observed in aromatic experiments. However, it also results in over-prediction of peak O_3 at the end of the experiment. This problem is particularly severe in MCMv3.1. Several theories have been proposed to resolve this issue and tested against chamber data to explain the high concentrations of OH radicals that lead to the aromatic decay without undergoing NO to NO_2 conversion [32], however, this remains a problem to be confirmed experimentally for aromatics.

3.4.2. VOC Mixtures

Experiments with VOC mixtures fully test the interactions between individual components of each mechanism. For VOC mixture experiments in the UNC chamber, peak O_3 is mostly over-predicted for all mechanisms (Figure 6 (a)). For MCMv3.1 a large overprediction is primarily influenced by the fast NO to NO_2 oxidation rate for aromatics.

The predicted NO, NO_2, and O_3 for individual VOC mixture experiments depend on the composition of the injected mixture for each mechanism and the injected VOC to NO_x ratio. For example, Figure 9 shows these profiles for two experiments, 3.0 ppmC SynIAG injected on one side of the chamber and 3.0 ppmC SynM85 injected on another side, with approximately 0.3 ppm NO_x. The solid observed lines clearly indicate SynIAG produces more O_3, most likely due to the larger carbon fractions of aromatics in SynIAG as

compared to SynM85 and the presence of highly reactive aldehydes in SynIAG mixture. For the SynIAG experiment, SAPRC07 performs well, but it overpredicts O_3 and underpredicts NO- NO_2 crossover times for the SynM85 experiment. For this reason, it is difficult to assess mechanism performance for VOC mixtures from the overall measures of results. Nevertheless, Figure 6 is a good indicator of mechanism performance across a range of VOC mixtures that might be present in an urban environment.

3.5. Conclusions

Seven gas-phase chemical mechanisms were compared against a large database of chamber data representing a variety of aromatic, ring-opening products, and VOC mixture experiments. The mechanisms use the reaction rate for the OH + NO_2 suggested by Mollner et al. (2010). The results from individual aromatic and ring-opening intermediate product experiments clearly show the need to include more explicit/semi-explicit representations of ring-opening products in any condensed mechanism. Without this representation it is likely not possible to capture the unique reactivity of individual carbonyl products.

Both SAPRC07 and MCMv3.1 largely over-predict peak O_3 and underpredict NO- NO_2 crossover times in aromatic and VOC mixture experiments. Both these mechanisms also over-predict the absolute NO degradation slope and NO_2 rise slope. This suggests faster and earlier NO to NO_2 oxidation rate. One possibility discussed in the literature is the regeneration of OH without NO to NO_2 conversion [21]. This pathway can help reduce peak O_3 and NO to NO_2 oxidation rate discrepancies. For CB mechanisms, it is hard to make general conclusions about mechanism deficiencies since they are highly tuned to predict O_3 in VOC mixtures. CB05TU is highly reactive earlier in the day, leading to large underprediction of NO- NO_2 crossover times. Results from CB05RMK validate the need for additional open-ring species in current CB mechanisms. This can also be useful for secondary organic aerosol prediction as shown by Kamens et al. (2011). In summary, all mechanisms except MCMv3.1 manage to predict the median of peak O_3 with a relative error less than 25%, for both aromatic and VOC mixtures. Although MCMv3.1 largely overpredicts peak O_3, it does relatively better in predicting the peak NO_2 compared to other mechanisms.

This analysis shows that different and widely-accepted methods for representing aromatic photochemistry in regulatory and research models can have significant effects on the evolution of ozone and NO_x concentrations. The experiments in this manuscript were not at ambient conditions, but instead were designed specifically to test the chemistry of several chemical mechanisms. The use of larger than ambient initial amounts of NO_x in the chambers allows for all day oxidation. In each experiment the terminal phase (e.g., removal of all reactive NOx) is reached late in the day as the actinic flux was declining. Thus, these experiments are a real challenge for these mechanisms to simulate the midday propagation period when the transition from the initial reactants to the primary products occur providing new radicals via photolysis processes at high actinic fluxes. These experiments are an indicator of the ability of the mechanism to simulate chemistry in air quality models.

Additional analyses need to be conducted to understand how these different

representations of aromatics might affect concentrations in ambient atmospheric conditions, although the uncertainty in these uncontrolled simulations will make it difficult to accurately evaluate them. The atmospheric chemistry of aromatic compounds remains an area of huge uncertainty, which requires additional research before we can confidently understand how to best represent it in air quality models.

Acknowledgments

This research was supported in part by the U.S. Environmental Protection Agency (UNC Contract No. EP-W-09-023). The authors thank all the past graduate students at University of North Carolina for conducting smog chamber experiments and providing a rich dataset to evaluate chemical mechanisms.

Disclaimer

Although this paper has been reviewed by EPA and approved for publication, it does not necessarily reflect EPAs policies or views.

Figure and Table Captions

Figure 1: Observed and modeled O_3, NO, and NO_2 mixing ratios for a toluene experiment conducted on August 1, 1983. The plots also show the total modeled nitrate.

Figure 2: Observed and modeled O_3, NO, and NO_2 mixing ratios for o-xylene experiment conducted on August 1, 1983. The plots also show the total modeled nitrate from all mechanisms except MCMv31.

Figure 3: Observed and modeled O_3, NO, and NO_2 mixing ratios for 1,3,5-trimethylbenzene experiment conducted on August 3, 1995. The dashed lines represent the modeling results and the solid lines represent observed data. The plots also show the total modeled nitrate from all mechanisms except MCMv31.

Figure 4: Observed and modeled toluene, o-xylene and 1,3,5-TMB mixing ratios for three experiments. The dashed lines represent the modeling results and the solid lines represent observed data.

Figure 5: Overall measures of results for all aromatic experiments. All the above indicated measures are reported in the form of relative error computed using Equation 2.

Figure 6: Overall measures of results for all VOC mixture experiments. All the above indicated measures are reported in the form of relative error computed using Equation 2.

Figure 7: Observed and modeled O_3, NO, and NO_2 mixing ratios for 1,4-butenedial and 4-oxo-2-pentenal experiment conducted on June 18, 1998. The dashed lines represent the modeling results and the solid lines represent observed data.

Figure 8: Observed and modeled O_3, NO, and NO_2 mixing ratios for 4-oxo-2-pentenal

and 3-hexene-2,5-dione experiment conducted on July 2, 1998. The dashed lines represent the modeling results and the solid lines represent observed data.

Figure 9: Observed and modeled O_3, NO, and NO_2 mixing ratios for SynIAG and SynM85 VOC mixture experiment conducted on July 24, 1991. The dashed lines represent the modeling results for SAPRC07 mechanism and the solid lines represent observed data.

Table 1: Categorization of chamber experiments based on initial injections in the chamber.

Table 2: Auxiliary mechanism in the UNC chamber.

Supplemental Figure and Table Captions

Figure S1: Model predicted actinic flux inside the UNC chamber for June 26, 1997.

Figure S2: Model predicted photolysis rates inside the UNC chamber for June 26, 1997.

Figure S3: Definition of all metrics used to evaluate mechanism performance and appear in the bar plots.

Figure S4: Observed and modeled O_3, NO, and NO_2 for chamber characterization experiments of carbon monoxide.

Figure S5: Observed and modeled O_3, NO, and NO_2 for chamber characterization experiments of methane on August 10, 1992.

Figure S6: Observed and modeled O_3, NO, and NO_2 for chamber characterization experiments of methane on July 21, 1991.

Figure S7: Observed and modeled O_3, NO, and NO_2 for chamber characterization experiments of methane on September 7, 1990.

Figure S8: Observed and modeled O_3, NO, and NO_2 for chamber characterization experiments of formaldehyde (top) and ethene (bottom) methane on August 16, 1998.

Figure S9: Observed and modeled O_3, NO, and NO_2 for chamber characterization experiments of formaldehyde on July 8, 1986.

Figure S10: Observed and modeled O_3, NO, and NO_2 for chamber characterization experiments of acetaldehyde (top) and propene (bottom) on June 17, 1998.

Table S1: Carbon fractions of various alkanes, alkenes, carbonyls, and aromatics across different hydrocarbon mixtures injected in experiments conducted at the UNC outdoor chamber. For SynE85, carbon fractions are without ethyl alcohol.

Table S2: List of experiments that were performed at UNC chamber and modeled for this study.

Table S3: List of injected species not present in MCMv3.1 and closest surrogate species used to model MCMv3.1 in this study.

REFERENCES

[1]. S. Houweling, F. Dentener, J. Lelieveld. The impact of nonmethane hydrocarbon compounds on tropospheric photochemistry. *J Geophys Res-Atmos*. **1998** May 20;103(D9):10673-96.

[2]. J. G. Calvert, R. Atkinson, K. Becker, R. Kamens, J. H. Seinfeld, T. Wallington, G. Yarwood. The Mechanisms of Atmospheric Oxidation of Aromatic Hydrocarbons. New York: Oxford University Press; **2002**.

[3]. H. R. Cheng, H. Guo, S. M. Saunders, S. H. M. Lam, F. Jiang, X. M. Wang, I. J. Simpson, D. R. Blake, P. K. K. Louie, T. J. Wang. Assessing photochemical ozone formation in the Pearl River Delta with a photochemical trajectory model. *Atmospheric Environment*. **2010** Nov;44(34):4199-208.

[4]. M. Zavala, W. Lei, M. J. Molina, L. T. Molina. Modeled and observed ozone sensitivity to mobile-source emissions in Mexico City. *Atmos Chem Phys*. **2009**;9(1):39-55.

[5]. R. M. Kamens, H. F. Zhang, E. H. Chen, Y. Zhou, H. M. Parikh, R. L. Wilson, K. E. Galloway, E. P. Rosen. Secondary organic aerosol formation from toluene in an atmospheric hydrocarbon mixture: Water and particle seed effects. *Atmospheric Environment*. **2011** Apr;45(13):2324-34.

[6]. Y. Zhou, H. F. Zhang, H. M. Parikh, E. H. Chen, W. Rattanavaraha, E. P. Rosen, W. X. Wang, R. M. Kamens. Secondary organic aerosol formation from xylenes and mixtures of toluene and xylenes in an atmospheric urban hydrocarbon mixture: Water and particle seed effects (II). *Atmospheric Environment*. **2011** Jul;45(23):3882-90.

[7]. J. Lee-Taylor, S. Madronich, B. Aumont, A. Baker, M. Camredon, A. Hodzic, G. S. Tyndall, E. Apel, R. A. Zaveri. Explicit modeling of organic chemistry and secondary organic aerosol partitioning for Mexico City and its outflow plume. *Atmos Chem Phys*. **2011**;11(24):13219-41.

[8]. EPA. Health Effects Notebook for Hazardous Air Pollutants. 2013; Available from: http://www.epa.gov/ttn/atw/hlthef/hapindex.html.

[9]. M. C. Dodge. Chemical oxidant mechanisms for air quality modeling: critical review. *Atmospheric Environment*. **2000**;34(12-14):2103-30.

[10]. S. M. Saunders, M. E. Jenkin, R. G. Derwent, M. J. Pilling. Protocol for the development of the Master Chemical Mechanism, MCM v3 (Part A): tropospheric degradation of non-aromatic volatile organic compounds. *Atmos Chem Phys*. **2003** Feb 12;3:161-80.

[11]. M. E. Jenkin, S. M. Saunders, M. J. Pilling. The tropospheric degradation of volatile organic compounds: A protocol for mechanism development. *Atmospheric Environment*. **1997** Jan;31(1):81-104.

[12]. R. G. Derwent, D. S. Stevenson, W. J. Collins, C. E. Johnson. Intercontinental transport and the origins of the ozone observed at surface sites in Europe. *Atmospheric Environment*. **2004** Apr;38(13):1891-901.

[13]. R. G. Derwent, M. E. Jenkin, S. M. Saunders, M. J. Pilling, P. G. Simmonds, N. R. Passant, G. J. Dollard, P. Dumitrean, A. Kent. Photochemical ozone formation in north west Europe and its control. *Atmospheric Environment*. **2003** May;37(14):1983-91.
[14]. Q. Ying, J. Y. Li. Implementation and initial application of the near-explicit Master Chemical Mechanism in the 3D Community Multiscale Air Quality (CMAQ) model. *Atmospheric Environment*. **2011** Jun;45(19):3244-56.
[15]. W. P. L. Carter. Development of the SAPRC-07 chemical mechanism. *Atmospheric Environment*. **2010** Dec;44(40):5324-35.
[16]. M. W. Gery, G. Z. Whitten, J. P. Killus, M. C. Dodge. A Photochemical Kinetics Mechanism for Urban and Regional Scale Computer Modeling. *J Geophys Res*. **1989** 1989;94(D10):12925-56.
[17]. G. Yarwood, S. Rao, M. Yocke, G. Z. Whitten. Updates to the Carbon Bond Mechanism: CB05**2005**.
[18]. A. W. Birdsall, J. F. Andreoni, M. J. Elrod. Investigation of the Role of Bicyclic Peroxy Radicals in the Oxidation Mechanism of Toluene. *Journal of Physical Chemistry A*. **2010** Oct 7;114(39):10655-63.
[19]. G. Obermeyer, S. M. Aschmann, R. Atkinson, J. Arey. Carbonyl atmospheric reaction products of aromatic hydrocarbons in ambient air. *Atmospheric Environment*. **2009** Aug;43(24):3736-44.
[20]. J. Noda, R. Volkamer, M. J. Molina. Dealkylation of Alkylbenzenes: A Significant Pathway in the Toluene, o-, m-, p-Xylene plus OH Reaction. *Journal of Physical Chemistry A*. **2009** Sep 3;113(35):9658-66.
[21]. C. Bloss, V. Wagner, A. Bonzanini, M. E. Jenkin, K. Wirtz, M. Martin-Reviejo, M. J. Pilling. Evaluation of detailed aromatic mechanisms (MCMv3 and MCMv3.1) against environmental chamber data. *Atmos Chem Phys*. **2005** Mar 1;5:623-39.
[22]. X. Liu, H. E. Jeffries, K. G. Sexton. Atmospheric photochemical degradation of 1,4-unsaturated dicarbonyls. *Environmental Science and Technology*. **1999** 1999;33:4212-20.
[23]. X. Liu, H. E. Jeffries, K. G. Sexton. Hydroxyl radical and ozone initiated photochemical reactions of 1,3-butadiene. *Atmospheric Environment*. **1999** 1999;33:3005-22.
[24]. S. J. White, M. Azzi, D. E. Angove, I. M. Jamie. Modelling the photooxidation of ULP, ES and E10 in the CSIRO smog chamber. *Atmospheric Environment*. **2010** Dec;44(40):5375-82.
[25]. H. E. Jeffries, D. L. Fox, R. M. Kamens. Outdoor Smog Chamber Studies: Light Effects Relative to Indoor Chambers. *Environmental Science and Technology*. **1976** October, 1976;10(10):1006-11.
[26]. H. E. Jeffries, K. G. Sexton. The Relative Ozone Forming Potential of Methanol-Fueled Vehicle Emissions and Gasoline-Fueled Vehicle Emissions in Outdoor Smog Chambers, Final Report. bound report. Atlanta, GA, ME-1 CRCP;**1995** January, 1995.
[27]. H. E. Jeffries, K. G. Sexton, T. Morris, M. Jackson, R. G. Goodman, R. M. Kamens, M. S. Holleman. Outdoor Smog Chamber Experiments Using Automobile Exhaust. Research Triangle Park, N.C.: U.S. Environmental Protection Agency**1985** March 1985. Report No.: EPA/600/3-85/032.
[28]. H. Jeffries. UNC Solar Radiation Models: US EPA**1991** Contract No.: Technical Report CR813107, CR813964, and CR815779.

[29]. H. Jeffries, I. Voicu, K. Sexton. Experimental Tests of Reactivity and Re-evaluation of the Carbon Bond Four Photochemical Reaction Mechanism: US EPA**2002** Contract No.: Technical Report R828906.

[30]. G. Z. Whitten, G. Heo, Y. Kimura, E. McDonald-Buller, D. T. Allen, W. P. L. Carter, G. Yarwood. A new condensed toluene mechanism for Carbon Bond CB05-TU. *Atmospheric Environment*. **2010** Dec;44(40):5346-55.

[31]. W. P. L. Carter. Development of a condensed SAPRC-07 chemical mechanism. *Atmospheric Environment*. **2010** Dec;44(40):5336-45.

[32]. C. Bloss, V. Wagner, M. E. Jenkin, R. Volkamer, W. J. Bloss, J. D. Lee, D. E. Heard, K. Wirtz, M. Martin-Reviejo, G. Rea, J. C. Wenger, M. J. Pilling. Development of a detailed chemical mechanism (MCMv3.1) for the atmospheric oxidation of aromatic hydrocarbons. *Atmos Chem Phys*. **2005** Mar 1;5:641-64.

[33]. A. K. Mollner, S. Valluvadasan, L. Feng, M. K. Sprague, M. Okumura, D. B. Milligan, W. J. Bloss, S. P. Sander, P. T. Martien, R. A. Harley, A. B. McCoy, W. P. L. Carter. Rate of Gas Phase Association of Hydroxyl Radical and Nitrogen Dioxide. *Science*. **2010** Oct 29;330(6004):646-9.

[34]. J. P. Killus, G. Z. Whitten. Background Reactivity in Smog Chambers. *International Journal of Chemical Kinetics*. **1990** Jun;22(6):547-75.

[35]. F. Rohrer, B. Bohn, T. Brauers, D. Bruning, F. J. Johnen, A. Wahner, J. Kleffmann. Characterisation of the photolytic HONO-source in the atmosphere simulation chamber SAPHIR. *Atmos Chem Phys*. **2005** Aug 12;5:2189-201.

[36]. J. Zador, T. Turanyi, K. Wirtz, M. J. Pilling. Measurement and investigation of chamber radical sources in the European Photoreactor (EUPHORE). *J Atmos Chem*. **2006** Oct;55(2):147-66.

[37]. H. E. Jeffries, K. G. Sexton. The Relative Ozone Forming Potential of Methanol-Fueled Vehicle Emissions and Gasoline-Fueled Vehicle Emissions in Outdoor Smog Chambers, Final Report for the Coordinating Research council for Project No. ME-1. bound report. Atlanta, GA: Coordinating Research Council Project ME-1**1995** January, 1995.

[38]. W. P. L. Carter. Development of an Improved Chemical Speciation Database for Processing Emissions of Volatile Organic Compounds for Air Quality Models. 2011; Available from: http://www.engr.ucr.edu/~carter/emitdb/.

[39]. H. E. Jeffries, M. W. Gery, M. Kessler, K. G. Sexton. Morphecule Reaction Mechansims, Morpho, Allomorphic Simulation Software. *.pdf**1998** 1998.

[40]. H. E. Jeffries, M. W. Gery, W. P. L. Carter. Protocols for evaluating oxidant mechanisms for urban and regional models. Research Triangle Park, NC: U.S. Environmental Protection Agency**1992**.

[41]. J. Arey, G. Obermeyer, S. M. Aschmann, S. Chattopadhyay, R. D. Cusick, R. Atkinson. Dicarbonyl Products of the OH Radical-Initiated Reaction of a Series of Aromatic Hydrocarbons. *Environmental Science & Technology*. **2009** Feb 1;43(3):683-9.

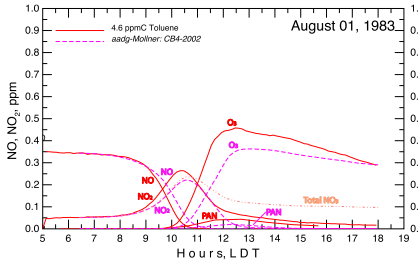

(a) CB4-2002

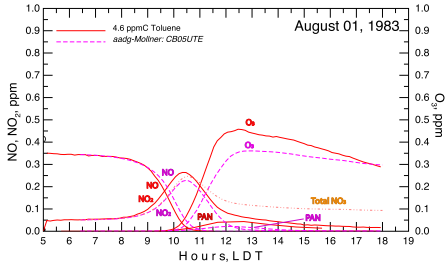

(b) CB05

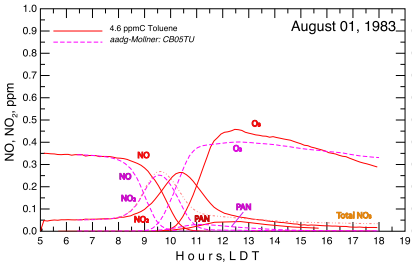

(c) CB05TU

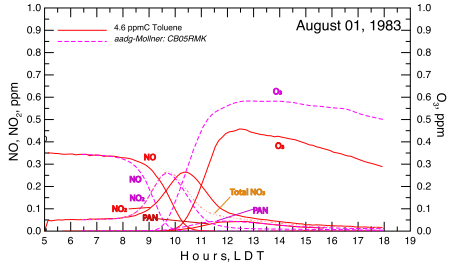

(d) CB05RMK

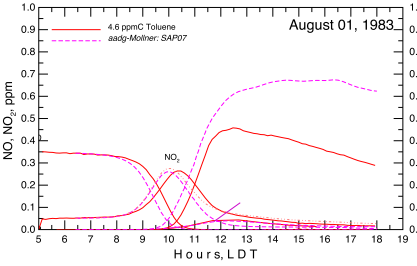

(e) SAPRC07

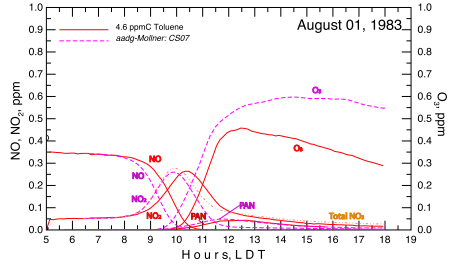

(f) CS07

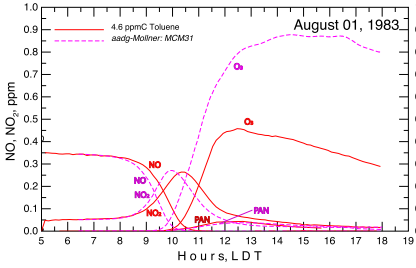

(g) MCMv3.1

Observed

Modeled

Modeled Total NO_3

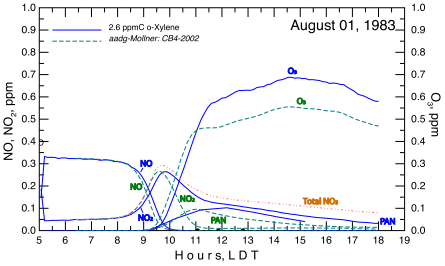

(a) CB4-2002

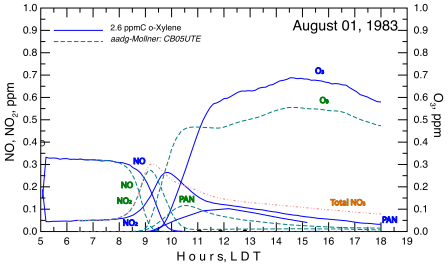

(b) CB05

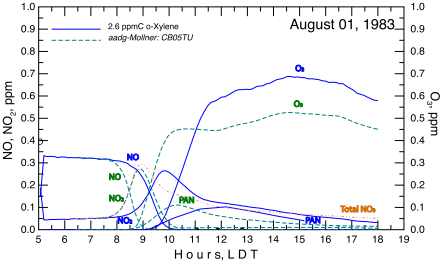

(c) CB05TU

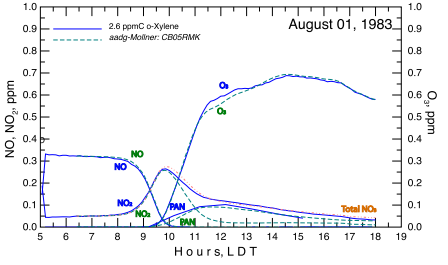

(d) CB05RMK

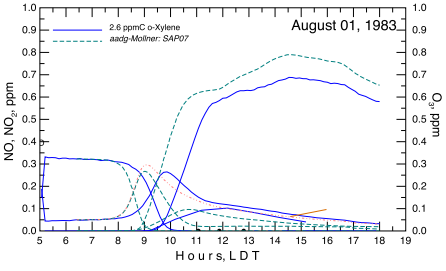

(e) SAPRC07

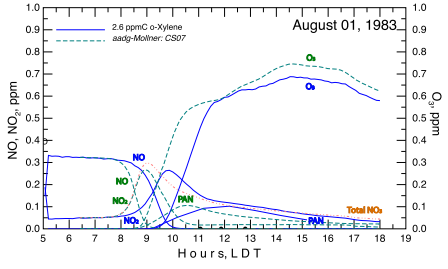

(f) CS07

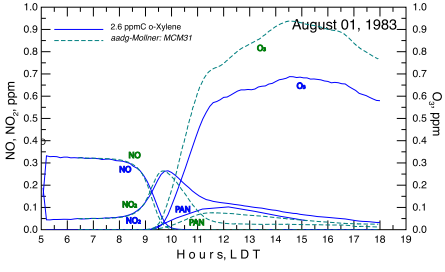

(g) MCMv3.1

Observed

Modeled

Modeled Total NO_3

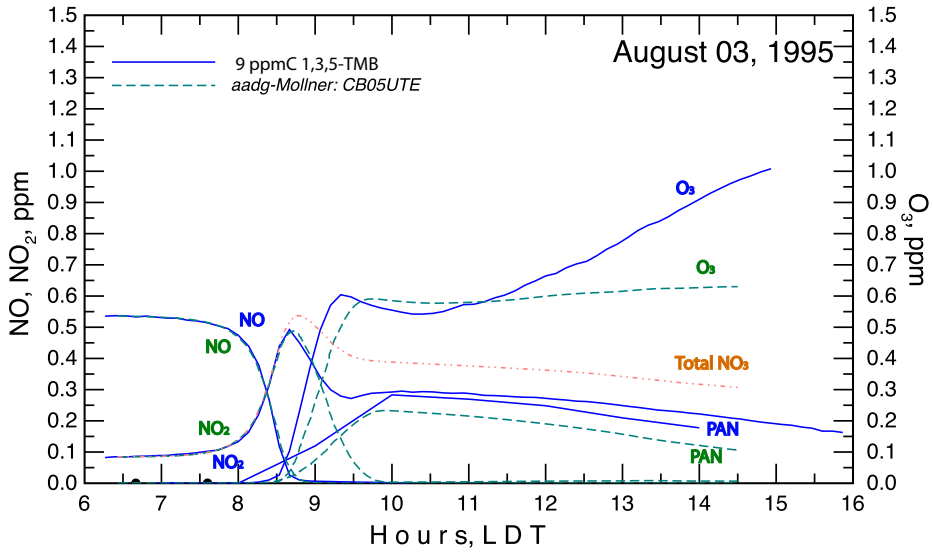

(a) CB05

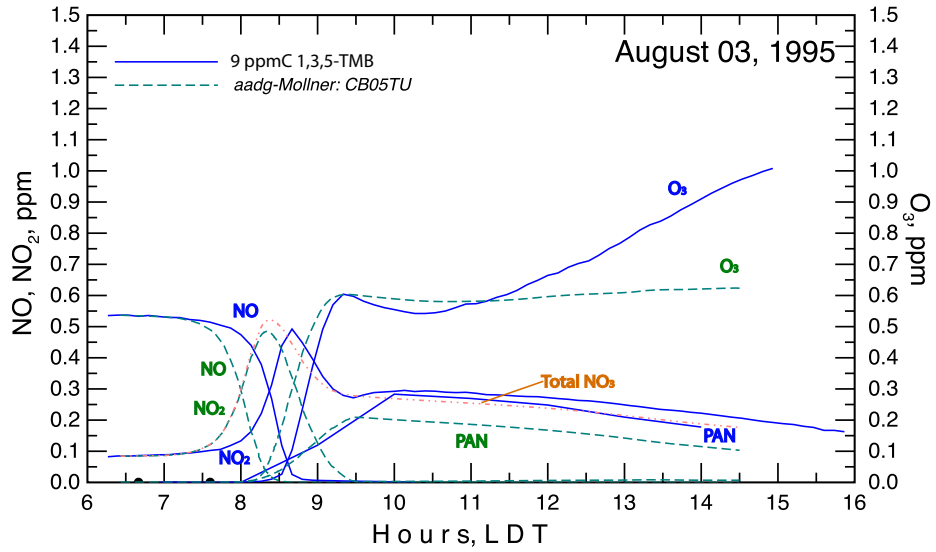

(b) CB05TU

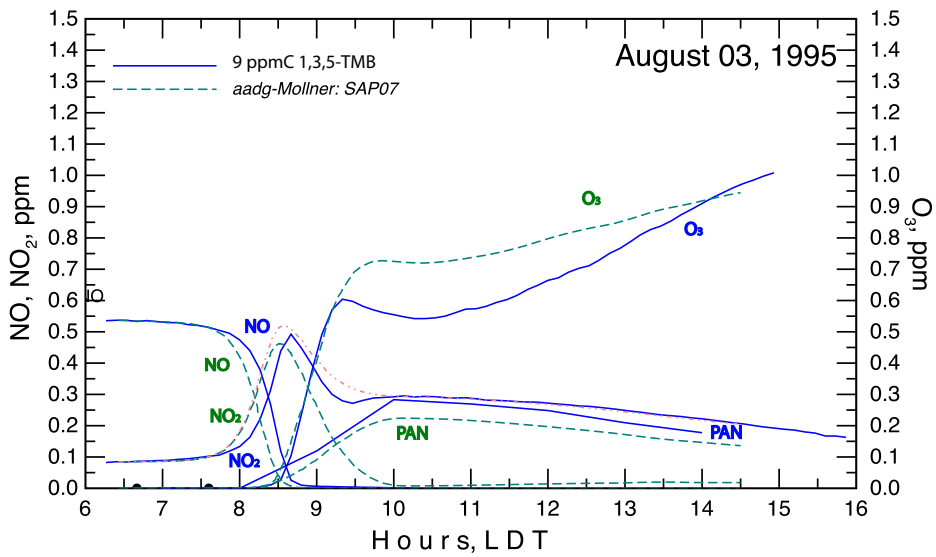

(c) SAPRC07

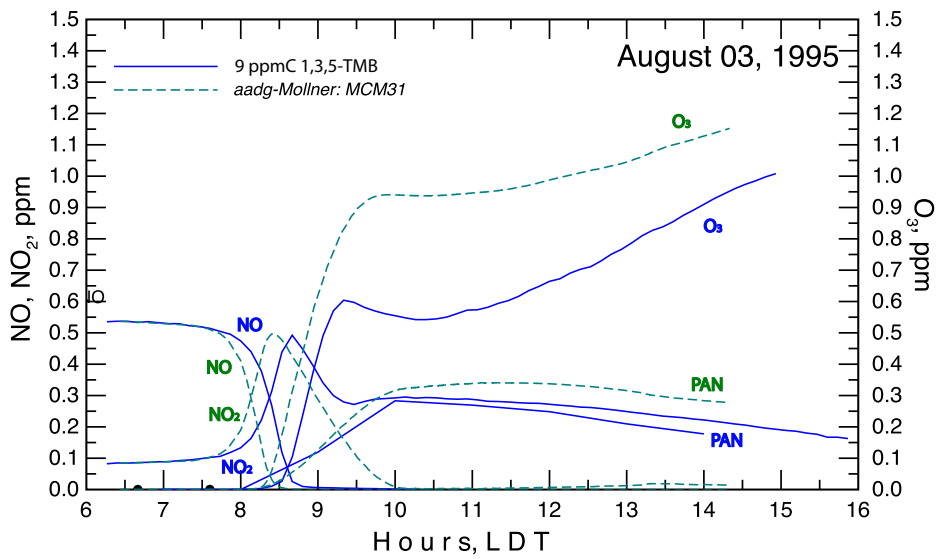

(d) MCMv3.1

Observed

Modeled

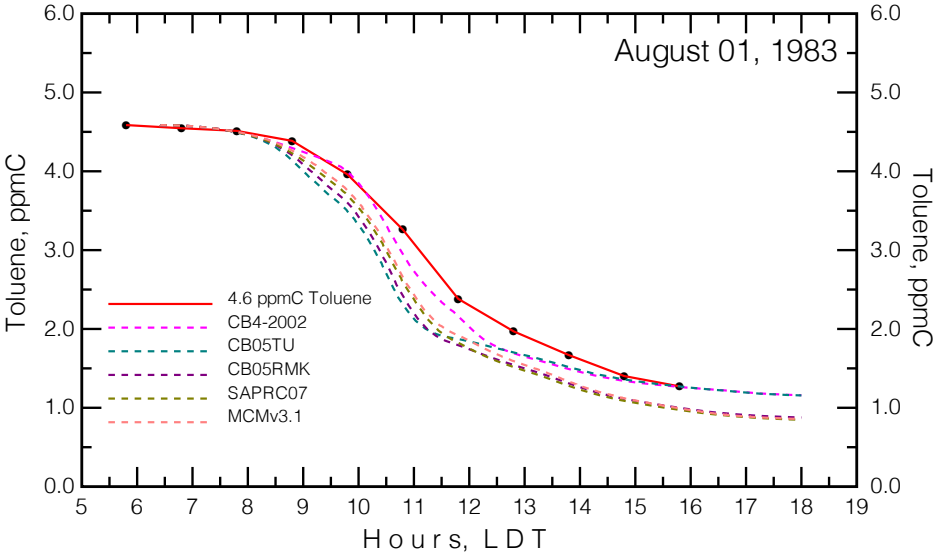

(a) 4 ppmC toluene/0.373 ppm NO_x

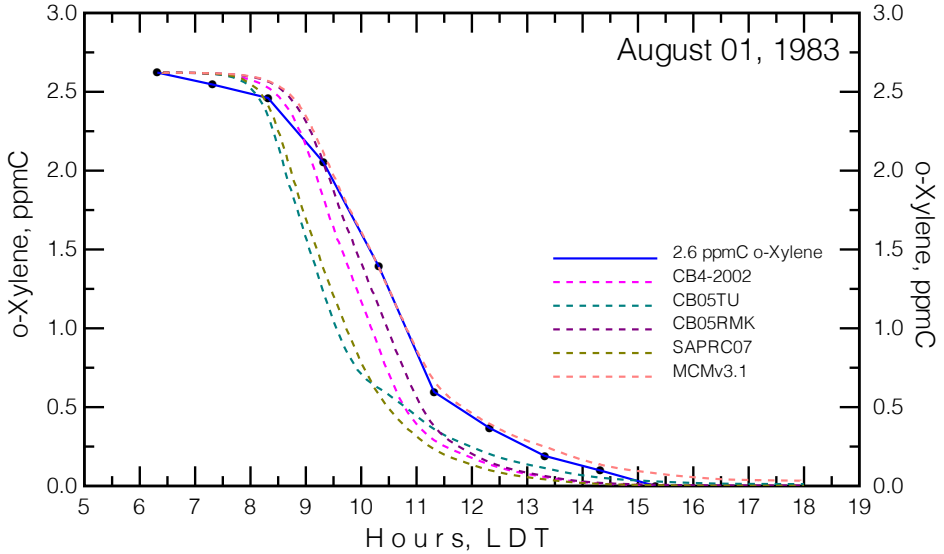

(b) 2.6 ppmC/0.373 ppm NO_x

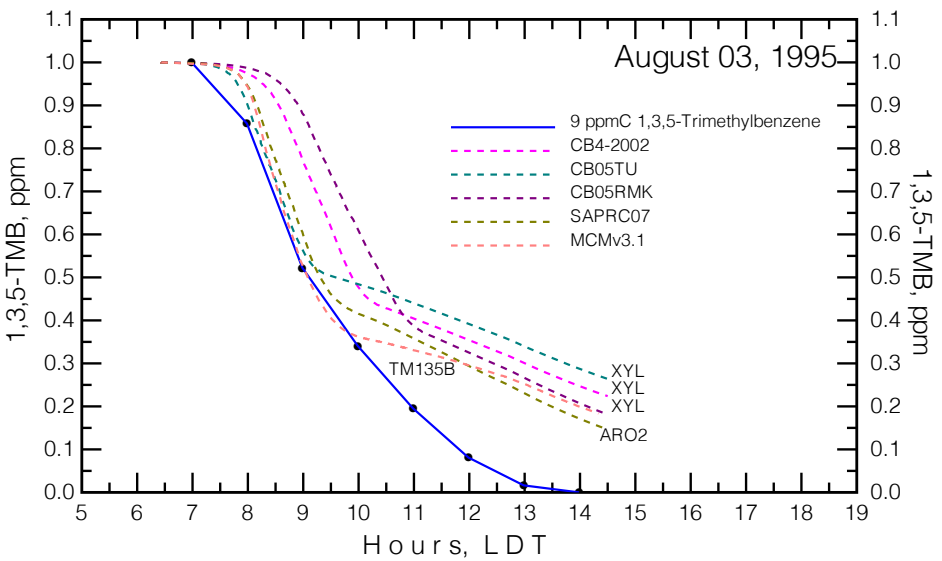

(c) 9 ppmC 1,3,5-TMB/0.629 ppm NO_x

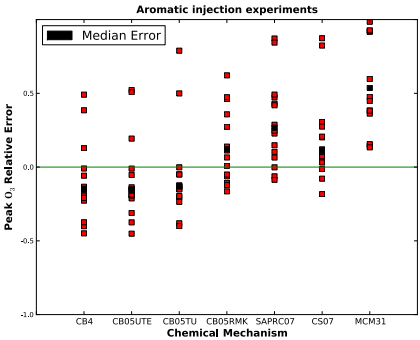
Aromatic injection experiments
Median Error
Peak O_3 Relative Error
0.5
0.0
-0.5
-1.0
CB4
CB05UTE
CB05TU
CB05RMK
SAPRC07
CS07
MCM31
Chemical Mechanism

(a)

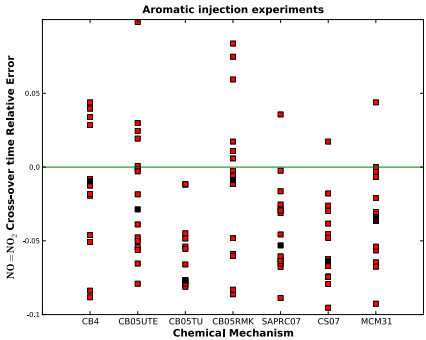
Aromatic injection experiments
$NO = NO_2$ Cross-over time Relative Error
0.05
0.0
-0.05
-0.1
CB4
CB05UTE
CB05TU
CB05RMK
SAPRC07
CS07
MCM31
Chemical Mechanism

(b)

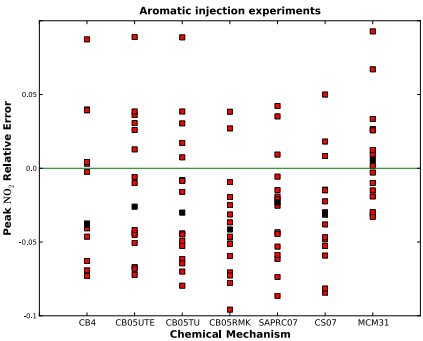
Aromatic injection experiments
Peak NO_2 Relative Error
0.05
0.0
-0.05
-0.1
CB4
CB05UTE
CB05TU
CB05RMK
SAPRC07
CS07
MCM31
Chemical Mechanism

(c)

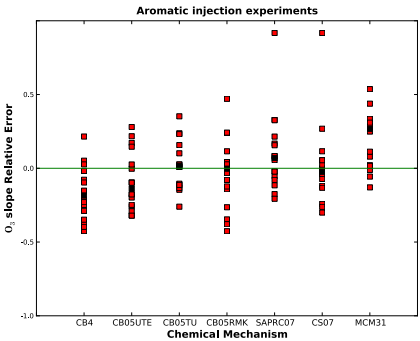
Aromatic injection experiments
O_3 slope Relative Error
0.5
0.0
-0.5
-1.0
CB4
CB05UTE
CB05TU
CB05RMK
SAPRC07
CS07
MCM31
Chemical Mechanism

(d)

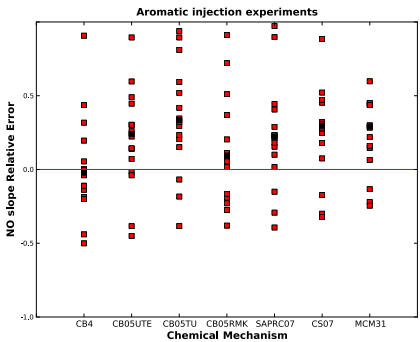
Aromatic injection experiments
NO slope Relative Error
0.5
0.0
-0.5
-1.0
CB4
CB05UTE
CB05TU
CB05RMK
SAPRC07
CS07
MCM31
Chemical Mechanism

(e)

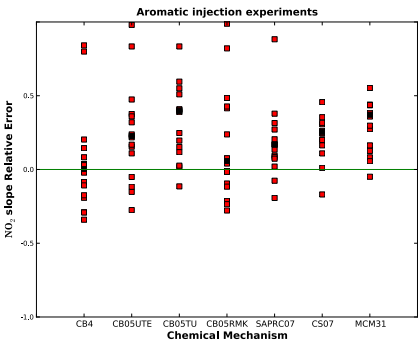
Aromatic injection experiments
NO_2 slope Relative Error
0.5
0.0
-0.5
-1.0
CB4
CB05UTE
CB05TU
CB05RMK
SAPRC07
CS07
MCM31
Chemical Mechanism

(f)

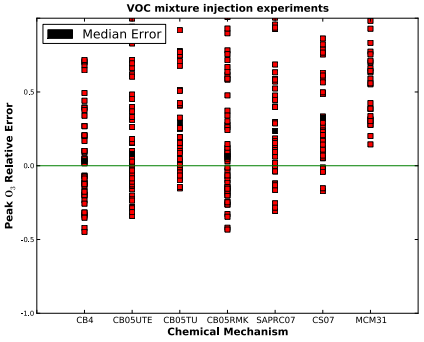
VOC mixture injection experiments
Median Error
Peak O_3 Relative Error
0.5
0.0
-0.5
-1.0
CB4
CB05UTE
CB05TU
CB05RMK
SAPRC07
CS07
MCM31
Chemical Mechanism

(a)

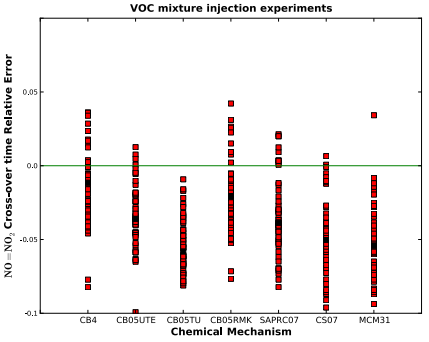
VOC mixture injection experiments
NO_2 Cross-over time Relative Error
0.05
0.0
-0.05
-0.1
CB4
CB05UTE
CB05TU
CB05RMK
SAPRC07
CS07
MCM31
Chemical Mechanism

(b)

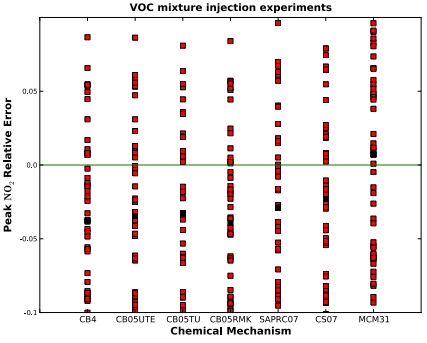
VOC mixture injection experiments
Peak NO_2 Relative Error
0.05
0.0
-0.05
-0.1
CB4
CB05UTE
CB05TU
CB05RMK
SAPRC07
CS07
MCM31
Chemical Mechanism

(c)

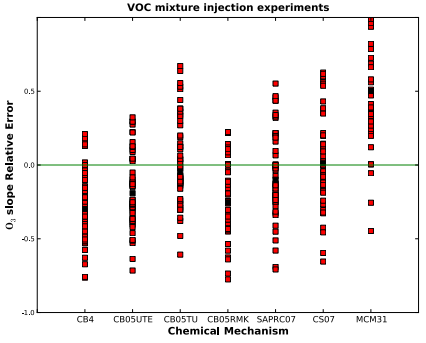
VOC mixture injection experiments
O_3 slope Relative Error
0.5
0.0
-0.5
-1.0
CB4
CB05UTE
CB05TU
CB05RMK
SAPRC07
CS07
MCM31
Chemical Mechanism

(d)

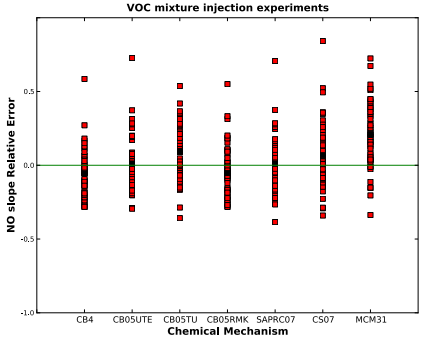
VOC mixture injection experiments
NO slope Relative Error
0.5
0.0
-0.5
-1.0
CB4
CB05UTE
CB05TU
CB05RMK
SAPRC07
CS07
MCM31
Chemical Mechanism

(e)

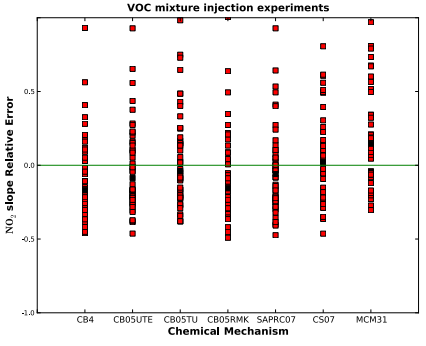
VOC mixture injection experiments
NO_2 slope Relative Error
0.5
0.0
-0.5
-1.0
CB4
CB05UTE
CB05TU
CB05RMK
SAPRC07
CS07
MCM31
Chemical Mechanism

(f)

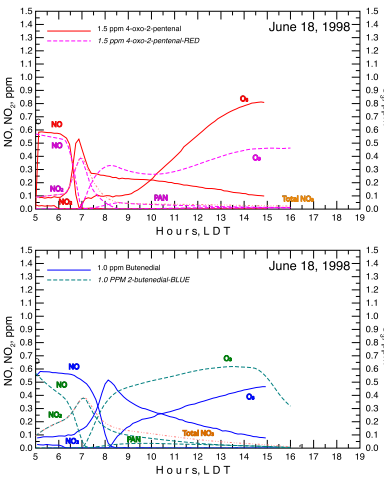

(a) CB05RMK

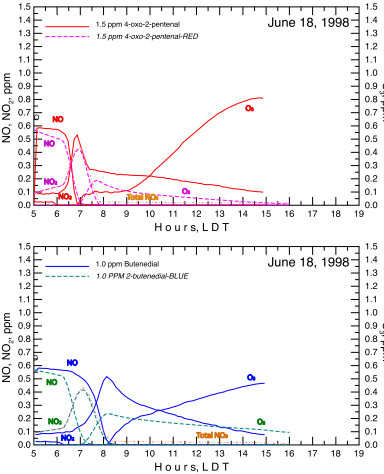

(b) CB05TU

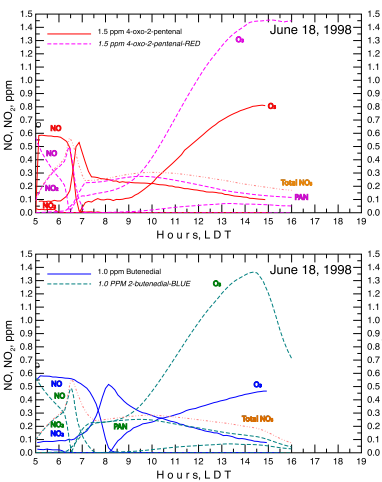

(c) SAPRC07

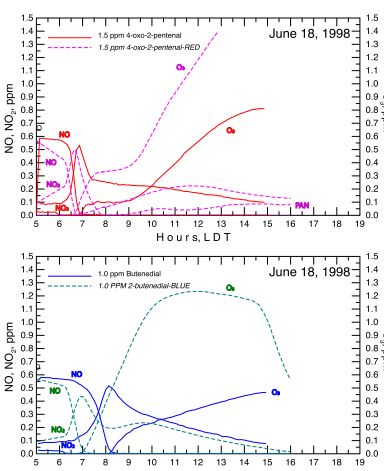

(d) MCMv3.1

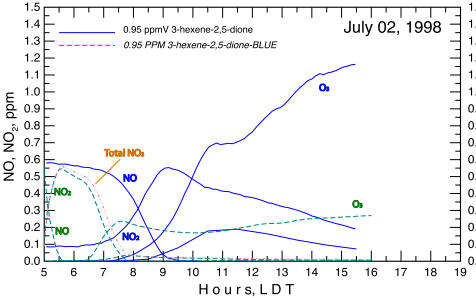

(a) CB05RMK

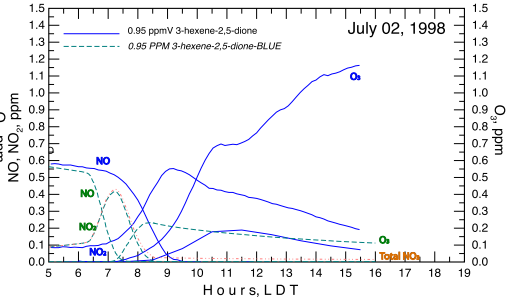

(b) CB05TU

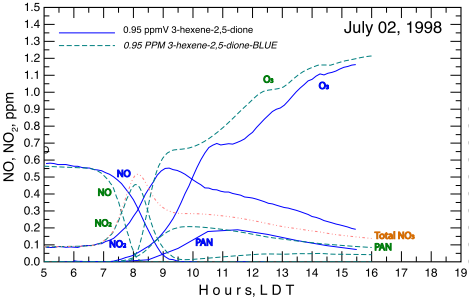

(c) SAPRC07

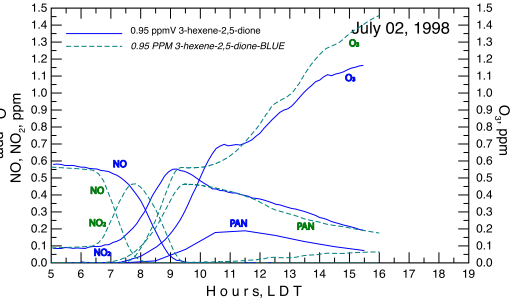

(d) MCMv3.1

Species/Mixtures[A]	Initial VOC:NOx[B]	Experiments[C]
Toluene	6-21	6
o/m/p-Xylene	2-13	5
1,3,5-TMB[D]	14	1
Toluene + p-Xylene +1,3,5-TMB	13	1
Butenedial	6	1
4-oxo-2-pentenal	6-11	2
3-hexene-2,5-dione	9	1
Toluene + UNCMIX80	9	1
m-Xylene + UNCMIX80	9	1
SynUrban	4-19	19
SynE85B + SynUrban	6	1
SynIAG	6-9	4
SynIAG + SynUrban	5-9	9
Isoprene + SynUrban	4	1
SynM85	6-9	3
SynM85 + SynUrban	5-8	4
SynE85E	6	1
SynE85E + SynUrban	5-6	3
SynE85E (minus EtOH)[E]+ SynUrban	6	1
SynCNG + SynUrban	9	1
Carter Mixture	6	1
SynLPG + SynUrban	6	1

[A]Initial injection species or mixture. Mixture compositions are reported in supplementary material.

[B]Ratio of initial VOC to NOx concentrations in the chamber. For multiple experiments in the same category, the range of VOC to

[C]Number of experiments performed in each category.

[D]1,3,5-TMB is 1,3,5-trimethylbenzene.

[E]SynE85E (minus EtOH) represents Synthetic E85 fuel mixture without ethyl alcohol.

› NOx ratio across all experiments in a particular category is reported.

No.	Reaction	Rate
	Background VOC[A]	
1	OH+BVOC➔0.667*CH3-OO· + 0.167*CH3-CO-OO·	$3x10^{-12}$ $MPCC^{-1}sec^{-1}$
	Deposition[B]	
2	H2O2	$6.7x10^{-4}$ sec^{-1}
3	O3	$2.3x10^{-6}$ sec^{-1}
4	N2O5➔2.0*WHNO3	$4.2x10^{-5}$ sec^{-1}
5	N2O5+WH2O➔2.0*WHNO3	$9x10^{-22}$ exp(2000/TK) $MPCC^{-1}sec^{-1}$
	Wall Partitioning[C]	
6	HNO3+WH2O➔WHNO3	$2.6x10^{-18}$ $MPCC^{-1}sec^{-1}$
7	WHNO3➔HNO3	$6.6x10^{-6}$ sec^{-1}
8	HONO+WH2O➔WHONO	$4.5x10^{-21}$ $MPCC^{-1}sec^{-1}$
9	WHONO➔HONO	$3.3x10^{-3}$ sec^{-1}
	NOx wall reactions[D]	
10	NO2+WH2O➔WNO2	$2.0x10^{-20}$ $MPCC^{-1}sec^{-1}$
11	WNO2➔NO2	$2.6x10^{-7}sec^{-1}$
12	WNO2+WNO2➔WN2O4	$2.0x10^{-15}$ $MPCC^{-1}sec^{-1}$
13	WN2O4+WH2O➔WHONO+WHNO3	$4.0x10^{-15}$ $MPCC^{-1}sec^{-1}$
14	NO+WHNO3➔1.0*HONO+1.0*NO2	$6.09x10^{-18}$ $MPCC^{-1}sec^{-1}$
15	NO2+WHNO3➔1.0*HONO+1.0*NO2	$3.38x10^{-19}$ $MPCC^{-1}sec^{-1}$
16	WHNO3+hv➔NO2	j(NO2 to O3P)*$8.0x10^{-5}$ sec^{-1}
17	NO2+hv➔HONO	j(NO2 to O3P)*0.0 sec^{-1}

[A]Background VOC represents the measured VOCs in the rural background air in Pittsboro, NC. The auxiliary mechanism treats this background mixture as a single model species that reacts with the ·OH radical.

[B]WHNO3 and WH2O represent the chamber wall nitric acid and wall water species

[C]WHONO represents the chamber wall HONO species.

[D]WNO, WNO2 and WN2O4 represent different chamber wall nitric oxides.